Ultraviolet photo-oxidation of polyvinylpyrrolidone (PVP) coatings on gold nanoparticles

Stacey M. Louie[1,2*], Justin M. Gorham[1], Jiaojie Tan[1], Vincent A. Hackley[1†]

[1]Materials Measurement Science Division, National Institute of Standards and Technology, Gaithersburg, MD 20899

[2]Department of Civil and Environmental Engineering, University of Houston, Houston, TX 77204

Co-corresponding authors:

[*]slouie@uh.edu

[†]vince.hackley@nist.gov

Submitted to *Environmental Science: Nano*

Abstract

Polymeric coatings are commonly applied to impart functionality and colloidal stability to engineered nanoparticles. In natural environments, transformations of the coating can modify the particle transport behavior, but the mechanisms and outcomes of these transformations have not yet been thoroughly evaluated. This study investigates the photo-transformations of polyvinylpyrrolidone (PVP) coatings on gold nanoparticles (AuNPs) under ultraviolet (UV) irradiation, representing light exposure in surface waters or other sunlit environments, and the impact on the AuNP colloidal stability. Multiple orthogonal characterization methods were applied to interrogate UV-induced transformations and their consequences. Rapid oxidation of the PVP coating occurred upon UV exposure. The transformed PVP largely persisted on the AuNP surface, albeit in a collapsed polymer layer around the AuNP surface. This transformation resulted in drastically diminished colloidal stability of the AuNPs, consistent with loss of steric stabilization. While the residual coating modified the interaction of the AuNPs with calcium counterions, it did not prevent subsequent stabilization by humic acid. This study demonstrates the importance of both chemical and physical coating transformations on nanoparticles, and hence the need for orthogonal and complementary characterization methods to fully characterize the coating transformations. Finally, the specific transformations of the PVP-coated AuNPs investigated here are discussed more broadly with respect to generalizability to other polymer-coated NPs and the implications for their fate in sunlit or other reactive environments.

Introduction

Polymeric coatings are ubiquitously applied to the surfaces of engineered nanoparticles (NP) to impart functionalities such as colloidal stability, resistance to protein adsorption, and targeted delivery for therapeutics.[1-5] Likewise, these surface coatings modify the fate and toxicity, and hence the potential implications or applications, of NPs in the natural environment.[1, 6] For example, for remediation of contaminated groundwater sites using "zerovalent" iron NPs, polymeric coatings are critical to minimize deposition and enhance transport of NPs through the subsurface, and they can also be designed to efficiently target the NP to organic/aqueous interfaces.[7-10]

In any environment, transformations of polymeric coatings on NPs can occur and significantly change the surface interactions and behavior of the NPs. Reactions of the coating can be induced by external agents in the environment (e.g., sunlight exposure, chemical redox agents, or biological activity) as well as by reaction with the NP itself (e.g., for redox-active or photoactive NPs). While transformations of the core metal or metal oxide NP have been probed in several prior studies,[11] relatively little is known about the pathways, rates, and effects of transformations of the polymeric coating itself, which can be centrally important in determining the environmental fate of the NPs.[1] Incidental transformations of the polymer coating can result in the loss of critical material functionalities, e.g. colloidal stability, which will directly impact the fate and transport of NPs. Alternatively, coating transformations could be intentionally exploited to develop stimuli-responsive polymeric coatings on NP surfaces. Here, we focus on photo-transformations that would occur in sunlit environments, e.g., surface waters receiving incidental releases of NPs[13-21] or foliar applications of NPs for agricultural use.[22-24]

Recently, our group demonstrated that degradation of thiolated methoxy polyethylene

glycol (mPEGSH) coatings on gold nanoparticles (AuNPs) occurs rapidly within 24 h under ultraviolet (UV) irradiation, resulting in diminished colloidal stability.[25] Notably, the surface coating transformation of mPEGSH observed on the AuNPs (loss of the ether chain but persistence of reduced thiolate groups) differed from the solution-phase reactions (thiol oxidation), emphasizing a critical need to analyze coating transformations directly on the NP surface. Additional coating types must be tested to identify a broader range of coating transformations that could occur, as well as to identify whether any generalizations can be made across coatings.

Here, the photo-transformation of polyvinylpyrrolidone (PVP) coatings are evaluated for AuNPs (60 nm nominal diameter). AuNPs were selected as a test NP to facilitate analysis of the coating transformations, because citrate-stabilized AuNPs are available in monodisperse suspensions and are colloidally stable under UV irradiation under the conditions tested here.[25] PVP was selected for investigation as a widely-used NP coating and an FDA-approved polymer.[5, 26] PVP coatings were previously postulated to degrade on Ag NPs under UV irradiation,[13] but direct analysis of the PVP surface coating on the NPs was not demonstrated. Pure PVP solutions and films (sans NPs) are also known to oxidize under UV light and other oxidizing conditions (e.g., sodium hypochlorite treatment of PVP/poly(ether sulfone) membranes)[27] to a variety of products, including succinimide and aspartic acid products[27, 28] and both chain scission[28] and crosslinking[29] products.

Considering the range of photo-oxidation products identified for pure PVP and our prior finding that surface-bound mPEGSH undergoes dissimilar transformations relative to dissolved mPEGSH,[25] the transformations of PVP coatings on AuNPs are not immediately predictable from prior studies on pure PVP. Furthermore, because colloidal stability depends on both layer conformation and chemistry,[6, 30-32] measurement of both physical and chemical changes may be

required to fully explain the impact of the coating transformation. Finally, the persistence or loss of transformation products on the NP surface may alter the interactions of the NP in environmental media, including its interactions with natural organic matter (NOM) (as explored previously for NPs with "pristine" coatings,[33-35] but not yet for those with transformed coatings). These particle-specific considerations are not relevant for dissolved PVP and represent novel contributions of this study.

Therefore, the primary objectives of this research are to characterize the photo-transformations of PVP coatings on AuNPs and to assess the effects on colloidal stability. To fully discern chemical transformations, conformational changes, and persistence of transformation products on the AuNP surface, complementary and orthogonal characterization methods are applied. These methods include particle sizing methods (dynamic light scattering (DLS) and electrospray–differential mobility analysis (ES-DMA)) and spectroscopic methods (UV-vis spectroscopy, attenuated total reflectance–Fourier transform infrared (ATR-FTIR) spectroscopy and X-ray photoelectron spectroscopy (XPS)). The effects of the transformations on the colloidal stability of the AuNPs are assessed in various environmental media, including those containing NOM, and correlated to the changes in the coating properties. Finally, we discuss the effects of coating preparation, NP type and size, and coating type and the broader implications for the fate of polymer-coated NPs in the environment.

Experimental

Materials and irradiation

Materials include citrate-stabilized AuNPs (cit-AuNPs) (60 nm nominal diameter) (BBI

Solutions, Cardiff, UK),[†] PVP (nominal 40 kDa) (Sigma Aldrich, St. Louis, MO), and polysuccinimide (PSI) (Lanxess, Pittsburgh, PA) to assist in identification of the PVP transformation products by XPS and FTIR. PVP-coated AuNPs (PVP-AuNPs) were prepared by mixing ≈ 28 mg L^{-1} of cit-AuNPs with 200 mg L^{-1} of PVP for (3 to 4) h and removing unadsorbed PVP by centrifugal ultrafiltration. Details are given in the Electronic Supporting Information (ESI). The PVP-AuNPs were resuspended in deionized (DI) water and used within 2 d of preparation. Fresh batches of cit-AuNPs were prepared with PVP coating for each replicate experiment. In addition to the PVP-AuNPs prepared in our lab, commercially available PVP-AuNPs with two nominal core sizes (NanoXact 30 nm PVP-AuNPs and NanoXact 60 nm PVP-AuNPs, Nanocomposix, San Diego, CA) were tested for comparison. Other materials are described in the ESI.

The washed PVP-AuNP suspensions (≈ 28 mg L^{-1} of Au) were irradiated in quartz vials for up to 24 h in a photoreactor (Rayonet RMR-600, Southern New England Ultraviolet Co. (SNEUCo) Branford, CT) equipped with a carousel and eight fluorescent lamps (RMR-3500A, SNEUCo) emitting UV light centered at 350 nm and ranging from (300 to 400) nm. The irradiance was estimated to be ≈ 30 W/m^2 by ferrioxalate actinometry, as described previously.[25, 36] Dark controls were wrapped in foil and held in the photoreactor simultaneously with the UV-exposed samples. The pH of the samples collected after 24 h was 6.8 ± 0.3 (n = 3 samples) and 6.8 ± 0.6 (n = 2) for the UV-exposed and dark NP suspensions, respectively.

Characterization

DLS and electrophoretic mobility (EM) measurements were performed on a Zetasizer

[†] The identification of any commercial product or trade name does not imply endorsement or recommendation by the National Institute of Standards and Technology.

Nano ZS (Malvern, Westborough, MA) after diluting the AuNP suspensions to ≈ 3 mg L^{-1} Au in 0.9 mmol L^{-1} $NaHCO_3$ (pH 8). Measurements and data analyses followed NIST-NCL Protocol PCC-1[37] and are described in our prior work[25] and the ESI. Asymmetric flow field-flow fractionation (AF4) coupled with on-line DLS was also performed, as described in the ESI.

For ES-DMA (ES: model 3480, TSI Inc., Shoreview, MN; DMA: model 3081 TSI Inc., Shoreview, MN), suspensions were concentrated to (550 to 600) mg L^{-1} of Au by centrifuging the AuNP suspensions (10 min at 1680 *g*, Eppendorf MiniSpin, Billerica, MA) and removing (90 to 95) mass % of the water and any dissolved salts or polymer. Further centrifugation steps were avoided to minimize NP aggregation. Prior to measurement, 10 µL of 20 mmol L^{-1} ammonium acetate was added to 40 µL of cleaned AuNP suspension, which ensures a stable electrospray condition. DMA was operated with a sheath flow of air (10 L min^{-1}) controlled by a mass flow controller (MKS Instruments, Andover, MA) and an aerosol flow of 1 L min^{-1} air controlled by the flowmeter in the ES device. A customized LabView program (National Instruments, Austin, TX) was used for control of electrical field applied to DMA and data acquisition by condensation particle counter (CPC, model 3776, TSI Inc., Shoreview, MN). A 0.5 nm step size was adopted for particle size measurement with a dwell time of 10 s at each step. A number-based particle size distribution was obtained by ES-DMA-CPC measurement. Detailed description of the ES-DMA principles can be found elsewhere.[38]

ATR-FTIR spectra were collected on cit-AuNP and PVP-AuNP samples (initial, 24 h UV, and 24 h dark) and the PVP and PSI polymers. 250 scans were collected at a resolution of 2 (data spacing 0.241 cm^{-1}) on a Nicolet Spectra 750 FTIR spectrometer (ThermoFisher Scientific) equipped with a Thunder Dome ATR attachment and diamond flat (ThermoFisher Scientific). For all samples, AuNP suspensions were washed four times by centrifuging to pellet and resuspending

in DI water. Onto the diamond crystal, ≈ 5 μL of concentrated suspension containing (25 to 30) μg of AuNPs was drop-cast. *In situ* UV exposure experiments were also performed by irradiation of a wet film of PVP-AuNPs on the diamond substrate under a Spectroline 4AW unit (Westbury, NY) equipped with one lamp (Rayonet RMR-3500A) providing 70 W m^{-2} irradiance (details in the ESI).

Samples for XPS were prepared by pelleting and rinsing the AuNP suspensions, depositing ≈ 200 μg of concentrated AuNPs suspension onto an ethanol-washed silicon substrate (University Wafers, Boston, MA), and drying under N_2 in a glove bag. High resolution XP spectra were acquired on an Axis Ultra DLD from Kratos Analytical, LTD (Chestnut Ridge, NY) using instrumental settings described previously[25] and in the ESI. Elements analyzed were O 1s, N 1s, C 1s, Si 2p, and Au 4f. Analysis of the spectra was accomplished using CasaXPS (Teignmouth, UK), as described in the ESI. All values reported are representative of the mean of at least 3 measurements ± 1 standard deviation, unless stated otherwise.

Agglomeration experiments

Time-resolved DLS[39, 40] was used to determine homo-agglomeration rates of the NPs in moderately hard water (MHW) (pH 7.9), artificial seawater (ASW) (pH 8.1), and a 100 mmol L^{-1} NaCl solution with 0.9 mmol L^{-1} $NaHCO_3$ (pH 8). Compositions of the MHW and ASW are reported in the ESI. The critical coagulation concentration (CCC) was determined for the cit-AuNPs and PVP-AuNPs (24 h UV or dark) in NaCl and $CaCl_2$ solutions. Interactions with NOM were assessed by incubating ≈ 23 mg L^{-1} of cit-AuNPs or PVP-AuNPs with 8 mg L^{-1} of Suwannee River Humic Acid (SRHA) (2S101H, International Humic Substances Society, St. Paul, MN) in DI water for 2 d, prior to determining CCCs in NaCl solution. For all measurements, the AuNP

concentration was ≈ 3 mg L^{-1}, and the concentrated salt solutions were added to the AuNP suspension and vortexed immediately prior to initiating DLS measurements. Measurements were collected at 1 min intervals for up to 20 min. Agglomeration rates were determined as the slope of a linear fit across only those data points where the mean *z*-average hydrodynamic diameter (d_z) was smaller than 1.3× the initial d_z, representative of dimer formation.[40] The attachment efficiency α was computed as the ratio of the measured agglomeration rate to the diffusion-limited agglomeration rate, and the CCC was estimated as the salt concentration to achieve $\alpha = 1$ from a linear fit of a log-log plot of α vs. salt concentration (below the CCC).[41]

Results and discussion

Physical transformations of hydrated PVP-AuNPs

The value of d_z determined by batch DLS for the AuNPs increased from (58.7 ± 0.9) nm with polydispersity index (PDI) of 0.15 ± 0.01 (n = 15) for the cit-AuNPs to (72.4 ± 3.3) nm with PDI of 0.15 ± 0.04 (n = 5) upon coating with PVP (Figure 1). No significant change in the agglomeration state of the NPs was observed upon coating with PVP and washing of excess PVP, as determined by AF4 with online DLS (ESI Figure S1) and indicated by the similar PDIs before and after coating and single decay observed in the autocorrelation plot (ESI Figure S2). Considering both the online and batch DLS results, the hydrodynamic thickness for the PVP layer is ≈ (2 to 7) nm. The EM became less negative after coating, which is likely attributable to a shift in the shear-plane away from the negatively-charged cit-AuNP surface and/or displacement of some citrate.

Both d_z and EM of the PVP-AuNPs decrease significantly during the first 9 h of UV exposure, with d_z reaching a statistically similar value to the uncoated cit-AuNPs within 24 h of

(58.6 ± 3.3) nm with PdI of 0.18 ± 0.03 (n = 5). The negative EM after irradiation may suggest remaining citrate on the AuNP surface. No significant change in either d_z or EM is observed for either the dark PVP-AuNP controls or the UV-exposed cit-AuNP controls. These results clearly indicate that UV exposure induces a physicochemical change in the PVP coating. Possible mechanisms consistent with the observed transformation include (1) physical loss of PVP from the AuNP surface, either by complete PVP desorption or scission and loss of polymer fragments (as previously observed by our group for mPEGSH-AuNPs[25]), or (2) chemical reaction of the PVP resulting in a conformational change in the PVP layer (i.e., shrinking of the layer around the AuNP surface). These mechanisms are distinguished by orthogonal measurements to evaluate changes in the chemistry, structure, and persistence of the PVP coating, presented hereafter.

Surface plasmon resonance (SPR)

UV-vis spectra (ESI Figure S3) show a SPR peak at 535 nm for the cit-AuNPs. SPR peak height and shape, which can be sensitive to the agglomeration state of the AuNPs, generally remained consistent upon coating of the AuNPs with PVP and UV exposure of the PVP-AuNPs, indicating minimal agglomeration of the NPs. The SPR peak wavelength is sensitive to the presence of surface coatings,[25, 42] and a (1 to 2) nm red-shift in the SPR peak was observed upon coating the cit-AuNPs with PVP. In our previous study, a blue shift in the SPR peak was observed upon UV-induced desorption of a PEG coating.[25] Here, no detectable blue shift in the SPR peak was observed after UV irradiation for PVP-AuNPs, suggesting persistence of a surface coating after transformation, as explored further with ATR-FTIR and XPS.

Surface chemistry transformations

Direct, quantitative characterization of surface composition is required to identify the chemical transformation of the PVP coating and the fate of the transformation products. Here, ATR-FTIR spectroscopy and XPS are used to evaluate the elemental composition at the PVP-AuNP surface and identify surface functional groups. For these measurements, all NPs were washed four times by centrifugation to pellet the NPs followed by resuspension in DI water to remove dissolved species, including any detached polymer.

ATR-FTIR spectra were collected both on dried deposits of NP or PVP samples that were prepared *ex situ*, as well as during an *in situ* UV irradiation experiment (Figure 2). For the as-prepared (0 h) and 24 h dark control PVP-AuNPs, the spectra obtained for the coating are consistent with those for the PVP control (Figure 2a). The peak at 1734 cm^{-1} is attributed to species adsorbed to the stock cit-AuNPs (ESI Figure S4) and is not considered in evaluation of the PVP transformations. Peaks for PVP and its oxidation products are assigned following previously reported asssignments.[28, 29, 43] After 24 h UV exposure, loss of the peaks for amide C=O stretching in PVP at 1683 cm^{-1} and pyrrolidone ring in-plane bending at 843 cm^{-1} is observed. Concomitantly, the formation of peaks for imide asymmetric and symmetric stretching at (1706 and 1768) cm^{-1}, respectively, and CH_2 twisting of the succinimide ring at 818 cm^{-1} was observed. These new peaks were not observed in the 0 h or 24 h dark PVP-AuNPs. Loss and formation of peaks in the fingerprint region were also observed after 24 h UV exposure. We speculate there is formation of a poly(vinyl succinimide) (PVS) product, which has been observed recently in the literature as a product of PVP 3-mer oxidized through other synthetic methods.[44] Since a PVS reference compound was not commercially available, the FTIR spectrum is presented for PSI as an imide reference and exhibits the two C=O stretching peaks representative of imides, similarly to the two

peaks observed for the PVP transformation product.

The *in situ* spectra (Figure 2b) were collected after UV exposure of PVP-AuNP deposits directly on the diamond ATR substrate under DI water, followed by drying of the sample. Wet samples were not analyzed directly because of overlap of the liquid water peak with the amide C=O peak. Amide oxidation was observed *in situ*, consistent with the *ex situ* results. The advantage of the *in situ* approach is that spectra can be compared directly before and after UV exposure to obtain the difference spectrum; however, dissolved oxygen and light penetration through the deposit may have been limited in the closed *in situ* system used here, resulting in incomplete reaction.

Overall, ATR-FTIR on the *ex situ* samples demonstrates the nearly-complete oxidation of the amide group in PVP to an imide group upon 24 h UV irradiation of the PVP-AuNPs. Furthermore, the observation of imide species in the spectra indicates that the transformed PVP product persists on the AuNP surface after washing the NPs (Figure 2a) or in an aqueous system where desorbed species can diffuse away from the ATR substrate (Figure 2b).

XPS was used to further characterize UV-induced chemical and elemental transformations. Acquisition of high resolution, low noise C 1s spectra and careful analysis of a comprehensive set of controls was essential to identify transformations in the PVP-AuNP samples from UV irradiation. The results of the peak fitted C 1s spectra for all PVP-AuNP experiments and controls are shown in Figure 3. Peak fitting assignments were determined from careful evaluation of the three controls, with five different functionalities of carbon extracted from these controls. The washed cit-Au control was characterized as an asymmetric line-shape with a peak maximum at 284.4 eV ± 0.1 eV. The entire spectrum was employed as a fit for the PVP-AuNP specimens (Figure 3(a); component 1) and is attributed to adventitious carbon with trace citrate contributions,

which was ubiquitous across all AuNP samples.

The PVP and PSI controls were employed to evaluate reactants and products, respectively, in the UV irradiated PVP-AuNP experiments. Each polymer control contributed three curves: two were the same functionality and one was unique to each polymer (Figure 3(b)). CC/CH_x and CN/CO peaks, peak fits 2 and 3, are representative of a hydrocarbon functionality and a carbon bound to 1 nitrogen, respectively. Hydrocarbon contributions are centered at 285.2 eV ± 0.1 eV, and C bound to 1 N only was set at 286.2 eV ± 0.1 eV. Additionally, PVP also has a carbon peak associated amide functionality (carbon type 4) located at 287.9 eV ± 0.0 eV while PSI has the imide type carbon (fit 5) present at 288.5 eV (n=1 for PSI).

All five functionalities were employed to fit all samples and controls to demonstrate the validity of the analysis. Figure 3(a) demonstrates that the fits for the PVP-AuNP samples accounted for the majority of the raw peak area. The distribution of C functionality remained unchanged between PVP-Au 0h and PVP-AuNP 24h dark specimens, suggestive that the polymer surface stabilizer remained chemically stable in the absence of light. Semi-quantitative assessment is shown in Figure 3c, which demonstrates that the sample's surface carbon remains comparable after 24 h in the dark with no statistically relevant change in amide functionality (11.5 % ± 0.3 % to 11.0 % ± 0.2 %). In contrast, UV exposure resulted in a much more dramatic loss in the amide signal, decreasing to 1.3 % ± 1.0 % for the PVP-AuNP 24 h UV sample. Concomitantly, the growth of the imide functionality occurred, increasing to 18.0 % ± 1.0 % from 1.0 % ± 0.3 % at 0.6 eV higher binding energy due to the increased electron withdrawing power of an additional oxygen on the 5-member ring. This also impacted the N 1s peak position by shifting from 399.9 eV ± 0.2 eV to 400.3 eV ± 0.1 eV after 24 h UV (data not shown).

Analysis of the surface elemental distributions for all samples and controls are presented

in Figure 4(a). The surfaces of the PVP-AuNP samples were dominated by Au, C, N and O signals with an absence of silicon (from the substrate) verifying the completeness of the NP deposit. Thus, we can assume all changes in the surface percentages of different elements are attributed to the AuNP, PVP, or adventitious carbon. The starting PVP-AuNP and the 24 h dark PVP-AuNP control showed no significant change in the distribution of surface elemental species. After 24 h UV irradiation, the oxygen concentration increased and the carbon concentration decreased, while the gold and nitrogen concentrations remained unchanged. This is more easily observed with the N:Au and O:Au ratios (Figure 4b) for different PVP-AuNP exposure conditions. Indeed, N:Au did not change for any of the specimens, in contrast with the O:Au ratio which increased after UV exposure. Overall, results presented in Figure 4 suggest the overall increase in oxidation of the PVP due to UV irradiation with some loss of carbon atoms and constant nitrogen contribution. This observation is consistent with the shift in the C1s spectra to reflect the formation of the imide carbon functionality in Figure 3 as well as the vibrational data in Figure 2(a).

Together, the ATR-FTIR and XPS measurements demonstrate oxidation of the amide group in the pyrrolidone ring of PVP to a succinimide group consistent with a PVS chemical structure shown in Figure 3b and consistent with intermediate oxidation products reported previously for pure PVP.[27, 28, 44] For chemical mechanisms, the reader is referred to pure PVP studies proposing oxidation to imides via formation of hydroperoxides.[27-29] PVP does not absorb UV-visible light at wavelengths > 300 nm, so it was previously speculated that impurities in the pure PVP samples initiated photooxidation. Here, irradiation of the AuNPs may result in generation of reactive oxygen species[45] that can contribute to photooxidation, as discussed later in this article. Pure PVP transformations could not be evaluated at the low concentrations expected to be adsorbed to the AuNPs; however, no significant change in size exclusion chromatograms

were observed for 100 mg L^{-1} PVP solutions after 7 d of UV irradiation either in the absence or presence of AuNPs, indicating the absence of detectable scission (data not shown).

On the AuNP surface, more extensive transformations beyond oxidation (e.g., hydrolysis or scission)[28] were not apparent within 24 h of UV irradiation. Furthermore, complete or nearly-complete persistence of the PVP-associated nitrogen on the AuNP surface was observed by XPS after transformation. Additionally, the constant N:Au ratio and Au% implies that the surface layer is characterized by a constant thickness or a relatively constant number of atoms at the AuNP surface with a different density.

Considering these results in the context of the decrease in hydrodynamic size measured by DLS, we deduce that oxidation of the pyrollidone groups in the PVP coating must result in a *conformational collapse* of the coating around the AuNP surface. This transformation can occur if intermolecular interactions change upon transformation of the PVP, i.e., if polymer↔polymer or polymer↔AuNP interactions become more favorable or if polymer↔water interactions become less favorable. We note that the dipole moment for succinimide[46] in the postulated product is lower than that of pyrrolidone,[47] and polysuccinimide has poor aqueous solubility[48] (<<1 g L^{-1} in our lab) whereas PVP has high solubility (>100 g L^{-1}).[49] We also emphasize that DLS measurements are performed under hydrated conditions, whereas XPS measurements are performed under vacuum. Therefore, we propose that the most likely mechanism for the collapse of the coating is expulsion of water from the coating due to unfavorable succinimide↔water interactions. In this case, minimal change in the *dry* layer thickness (as opposed to hydrated layer thickness in DLS) should be observed before and after the coating transformation; this hypothesis is evaluated by ES-DMA measurements, presented hereafter.

Size of aerosolized PVP-AuNPs

Size distributions for dry (aerosolized) NPs were obtained by ES-DMA (Figure 5). The peak diameters measured by ES-DMA indicate the as-prepared PVP-AuNPs are ≈ 2 nm larger than the cit-AuNPs, suggesting a *dry* layer thickness of ≈ 1 nm. Notably, no significant decrease in the diameter of the UV-exposed PVP-AuNPs is observed compared to that of the dark controls or as-prepared PVP-AuNPs. These results are consistent with the XPS results, showing minimal loss of coating from the AuNP surface, and they further support the proposed explanation that the decrease in hydrodynamic layer thickness observed by DLS reflects a collapse of the layer around the AuNP due to expulsion of water.

Effects on colloidal stability in environmental media

Photo-induced changes to the chemistry and structure of the PVP coating are expected to significantly affect the colloidal stability of the AuNPs. Colloidal stability was first compared for the PVP-AuNPs (24 h UV and 24 h dark) and cit-AuNPs in two environmentally relevant media, MHW and ASW, and in a 100 mmol L^{-1} NaCl solution with 1 mmol L^{-1} $NaHCO_3$ (pH 8) (ESI Figure S5). In ASW, all samples agglomerated rapidly over 10 min and no significant difference was observed among samples. In MHW, both the dark and UV-exposed PVP-AuNPs showed minimal agglomeration within 10 min, whereas cit-Au agglomerated rapidly, consistent with the persistence of coating after transformation. However, in 100 mmol L^{-1} NaCl (intermediate ionic strength between MHW and ASW), the UV-exposed PVP-AuNPs showed similar agglomeration rates to the cit-AuNPs, whereas the dark PVP-AuNP control showed minimal agglomeration, a result that is consistent with loss of steric stability upon collapse of the polymer layer.

Critical coagulation concentrations (CCC) were determined to quantitatively evaluate

differences in colloidal stability and the influence of Na^+ versus Ca^{2+} (Figure 6). The PVP-AuNPs after 24 h UV exposure (CCC = (80 ± 3) mmol L^{-1} NaCl, n = 3) behaved similarly to the cit-AuNPs (CCC = (80 ± 2) mmol L^{-1} NaCl, n = 2). On the other hand, the dark PVP-AuNP controls exhibited a CCC > 1 mol L^{-1} NaCl (not shown). These results again indicate nearly complete loss of steric stabilization in the presence of Na^+ counterion upon collapse of the PVP coating. However, in $CaCl_2$, the CCC of the UV-exposed PVP-AuNPs ((2.84 ± 0.02) mmol L^{-1} $CaCl_2$, n = 2) was higher than that of the cit-AuNPs ((2.00 ± 0.01) mmol/$CaCl_2$, n = 2). The mechanism for the difference in Ca^{2+} (but not Na^{2+}) interaction with the cit-AuNPs and transformed PVP-AuNPs was not directly investigated, but the results suggest a specific interaction beyond charge screening occurs with Ca^{2+}, possibly charge neutralization[21] upon complexation to form insoluble calcium citrate on the cit-AuNPs. The interaction between Ca^{2+} and citrate may be blocked by the presence of the oxidized PVP coating. These results explain differences in the agglomeration rates of UV-exposed PVP-AuNPs and cit-AuNPs in MHW, where Ca^{2+} is a significant counterion. Overall, results are consistent with expected electrostatic and steric stabilization mechanisms after accounting for the coating transformations.[6] More interestingly, these results demonstrate that persistence of transformation products results in a *distinct surface chemistry* with *distinct agglomeration behavior* for the UV-exposed PVP-AuNPs compared to the cit-AuNPs and as-prepared PVP-AuNPs.

In natural environments, NOM can adsorb to NPs and modify their colloidal stability. Polymeric coatings on the NP surface may block NOM adsorption; therefore, we investigated the agglomeration of the UV-exposed PVP-AuNPs and cit-AuNPs after equilibration in SRHA-containing medium. SRHA imparted additional colloidal stability to both the cit-AuNPs and UV-exposed PVP-AuNPs (Figure 6a), indicating that the transformed PVP layer does not prevent

SRHA interaction with the AuNPs. This result is consistent with prior studies that found that humic or fulvic acids interact even with as-prepared PVP-AuNPs.[33, 34] This result also suggests that interactions of uncoated NPs with NOM may ultimately be a sufficient scenario to assay for long-term predictions of NP fate in the environment, because the initial polymeric coating can transform or degrade over time and hence play a less important role than subsequent adsorption of NOM.

Generalizability of photo-transformations

Further questions arise regarding the generalizability of the results observed for the specific set of PVP-AuNPs tested here to other NPs of different size, coating preparation (e.g., protocol and resulting ligand density), NP core material, and coating material. In this study, we evaluated the photo-transformations of commercially available PVP-AuNPs of two nominal core diameters (30 nm and 60 nm) that were purchased with the PVP coating in place, rather than prepared by adsorbing PVP to cit-AuNPs in our lab. The same general trend of decreasing hydrodynamic size with UV exposure time was observed for the commercially available PVP-AuNPs (ESI Figure S6) as for the cit-AuNPs that were coated with PVP in our lab, indicating that this result can be generalized to other PVP-AuNPs regardless of AuNP core size or ligand density (which may vary with the coating procedure). However, for the commercial 60 nm PVP-AuNPs tested under the same conditions as those prepared in our lab, the hydrodynamic size equilibrated after a longer UV exposure duration (72 h). The slower time to equilibration for the commercial 60 nm PVP-AuNPs compared to those prepared in our lab could be consistent with a higher ligand density on the commercial PVP-AuNPs, although ligand densities were not directly measured here.

With respect to the effect of the NP core material (specifically, its photoreactivity), a prior

study observed singlet oxygen ($^1O_2$) generation in aqueous suspensions of 20 nm AuNPs under UV irradiation (similarly with Si and Ni nanoparticles),[45] but no generation of superoxide radical ($O_2^{\bullet-}$) or more highly reactive hydroxyl radicals ($^{\bullet}OH$) by AuNPs (as opposed to significant generation of these species by Ag, TiO_2, and ZnO NPs).[45, 50] Generation of reactive oxygen species (ROS) by AuNPs under X-ray exposure has been reported to be size dependent,[51] with decreased photoreactivity as size increases. As such, the 60 nm AuNPs could have contributed to induce the oxidation of the PVP coating, but faster oxidation rates would be expected on more highly photoreactive NPs and slower rates comparable to those in pure PVP studies[28] on nonreactive NPs.

Clearly, we expect that photo-transformations will depend on the polymer material itself, but if all transformations led to the same end result (e.g., loss of polymer from the NP surface), testing requirements could be simplified. However, comparison of the results of this study on PVP-AuNPs to our parallel study on mPEGSH-AuNPs[25] (Table 1) demonstrates that such simplifying assumptions are not appropriate. Some similarities in transformations were observed, i.e., the hydrodynamic thickness of both coatings decreased upon UV exposure, resulting in diminished colloidal stability. However, persistence of the oxidized product differed considerably for the two polymers: significant loss of the PEG chain was observed (leaving a smaller residual thiolate component), in contrast to the nearly-complete persistence of the oxidized PVP product (albeit in a collapsed form). Hence, with only two test cases, we observe fundamentally different end results that suggest that coating transformations will need to be evaluated on a case-by-case basis.

The ability to predict the transformations of the polymer coating from studies on pure polymers would be of high interest, as it could minimize the need to characterize the coating transformations directly on the NP. However, for both the PVP and mPEGSH coatings, the

expected endpoint of the reaction (hydrolysis of PVP, or oxidation of thiolate from the mPEGSH-AuNP surface) was not observed within 24 h of UV exposure. Because intermediate reaction products were important, coating transformations and their effects would be difficult to predict *a priori* from studies on pure polymers. Finally, we emphasize that persistence and conformational changes of the coating are especially important in determining the steric interactions of the NPs, and these physical transformations of the adsorbed layer would not be straightforward to predict from pure polymer studies.

Conclusions and Implications

UV irradiation induces significant oxidation of PVP coatings on AuNPs, which further results in collapse to a denser, less hydrated coating. Colloidal stability of the NPs decreases drastically upon loss of steric stabilization compared to the as-prepared PVP-AuNPs, but the presence of residual transformation products results in different interactions of the transformed PVP-AuNPs with Ca^{2+} that cannot be predicted from the cit-AuNPs. However, the residual coating does not interfere significantly with the ability of NOM to sorb and impart colloidal stability. Ultimately, the agglomeration behavior for this complex system (UV-irradiated PVP-coated AuNPs in HA-containing waters) may be reasonably predicted by a simpler surrogate system (cit-AuNPs with HA) for this specific coating. Further studies should probe whether other aspects of the NP behavior (reactivity, toxicity) are altered significantly upon PVP oxidation, or whether heterogeneity of the coating (mixtures of pristine and transformed polymer and NOM) impacts NP fate.[33, 34, 52, 53]

Future research efforts can apply knowledge of coating transformations to improve the design of nanomaterials for environmental safety or for environmental applications. For example,

using coatings that can transform rapidly, as observed for PVP and mPEGSH or potentially for other coatings of higher lability, may be beneficial if poorer mobility of the NPs in the water column reduces exposure and hence environmental risk. "Smart" coatings can also be envisioned, in which an environmental stimulus triggers a transformation of the polymer for a desired function such as slow release.[12] Prediction or control of the fate of polymer-coated NPs for environmental implications or applications will ultimately rely on a sound fundamental understanding of the chemical and physical transformations of the surface coating, which will require thorough characterization of the coating transformations as demonstrated here using a suite of orthogonal methods.

Electronic Supporting Information Available

Additional methods and results for AF4-DLS, SPR, ATR-FTIR, aggregation experiments, and commercial PVP-AuNPs are presented in the electronic supporting information.

Acknowledgments

We thank Richard Gates for use of the ATR-FTIR instrument, Jeffrey Clogston for size exclusion chromatography (SEC) measurements, the National Research Council for a postdoctoral fellowship to SML, and the nanoEHS initiative program at NIST, coordinated by Debra Kaiser, for providing long term funding support that in part enabled this study.

References

1. S. M. Louie, R. D. Tilton and G. V. Lowry, *Environ. Sci.: Nano*, 2016, **3**, 283-310.
2. A. E. Nel, L. Madler, D. Velegol, T. Xia, E. M. V. Hoek, P. Somasundaran, F. Klaessig, V. Castranova and M. Thompson, *Nat. Mater.*, 2009, **8**, 543-557.
3. H. Otsuka, Y. Nagasaki and K. Kataoka, *Adv. Drug Deliver. Rev.*, 2003, **55**, 403-419.
4. J. W. Krumpfer, T. Schuster, M. Klapper and K. Mullen, *Nano Today*, 2013, **8**, 417-438.
5. T. M. Tolaymat, A. M. El Badawy, A. Genaidy, K. G. Scheckel, T. P. Luxton and M. Suidan, *Sci. Total Environ.*, 2010, **408**, 999-1006.
6. A. R. Petosa, D. P. Jaisi, I. R. Quevedo, M. Elimelech and N. Tufenkji, *Environ. Sci. Technol.*, 2010, **44**, 6532-6549.
7. T. Phenrat, N. Saleh, K. Sirk, H. J. Kim, R. D. Tilton and G. V. Lowry, *J Nanopart Res*, 2008, **10**, 795-814.
8. F. He and D. Y. Zhao, *Environ. Sci. Technol.*, 2007, **41**, 6216-6221.
9. C. M. Cirtiu, T. Raychoudhury, S. Ghoshal and A. Moores, *Colloid Surface A*, 2011, **390**, 95-104.
10. N. Saleh, K. Sirk, Y. Q. Liu, T. Phenrat, B. Dufour, K. Matyjaszewski, R. D. Tilton and G. V. Lowry, *Environ Eng Sci*, 2007, **24**, 45-57.
11. G. V. Lowry, K. B. Gregory, S. C. Apte and J. R. Lead, *Environ Sci Technol*, 2012, **46**, 6893-6899.
12. S. M. Rodrigues, P. Demokritou, N. Dokoozlian, C. O. Hendren, B. Karn, M. S. Mauter, O. A. Sadik, M. Safarpour, J. M. Unrine, J. Viers, P. Welle, J. C. White, M. R. Wiesner and G. V. Lowry, *Environ. Sci.: Nano*, 2017, **4**, 767-781.
13. S. J. Yu, Y. G. Yin, J. B. Chao, M. H. Shen and J. F. Liu, *Environ. Sci. Technol.*, 2014, **48**, 403-411.
14. J. M. Gorham, R. I. MacCuspie, K. L. Klein, D. H. Fairbrother and R. D. Holbrook, *J Nanopart Res*, 2012, **14**.
15. Y. W. Cheng, L. Y. Yin, S. H. Lin, M. Wiesner, E. Bernhardt and J. Liu, *J Phys Chem C*, 2011, **115**, 4425-4432.
16. C. W. Isaacson and D. C. Bouchard, *Environ Sci Technol*, 2010, **44**, 8971-8976.
17. W. C. Hou, C. J. He, Y. S. Wang, D. K. Wang and R. G. Zepp, *Environ Sci Technol*, 2016, **50**, 3494-3502.
18. Y. Yin, X. Yang, X. Zhou, W. Wang, S. Yu, J. Liu and G. Jiang, *J Environ Sci (China)*, 2015, **34**, 116-125.
19. Q. Zheng, M. Zhou, W. Deng and X. Chris Le, *J Environ Sci (China)*, 2015, **34**, 259-262.
20. Z. L. Hua, J. A. Zhang, X. Bai, Z. F. Ye, Z. Q. Tang, L. Liang and Y. Q. Liu, *Sci. Total Environ.*, 2016, **539**, 196-205.
21. X. L. Qu, Y. S. Hwang, P. J. J. Alvarez, D. Bouchard and Q. L. Li, *Environ. Sci. Technol.*, 2010, **44**, 7821-7826.
22. W. H. Elmer and J. C. White, *Environ. Sci.: Nano*, 2016, **3**, 1072-1079.
23. J. Hong, J. R. Peralta-Videa, C. Rico, S. Sahi, M. N. Viveros, J. Bartonjo, L. Zhao and J. L. Gardea-Torresdey, *Environ Sci Technol*, 2014, **48**, 4376-4385.
24. M. Borisev, I. Borisev, M. Zupunski, D. Arsenov, S. Pajevic, Z. Curcic, J. Vasin and A. Djordjevic, *PLoS One*, 2016, **11**, e0166248.
25. S. M. Louie, J. M. Gorham, E. A. McGivney, J. Y. Liu, K. B. Gregory and V. A. Hackley, *Environ. Sci.: Nano*, 2016, **3**, 1090-1102.

26. L. D. Pachon and G. Rothenberg, *Appl. Organomet. Chem.*, 2008, **22**, 288-299.
27. Y. Hanafi, A. Szymczyk, M. Rabiller-Baudry and K. Baddari, *Environ. Sci. Technol.*, 2014, **48**, 13419-13426.
28. F. Hassouna, S. Therias, G. Mailhot and J. L. Gardette, *Polym. Degrad. Stabil.*, 2009, **94**, 2257-2266.
29. X. F. Zhu, P. Lu, W. Chen and J. A. Dong, *Polymer*, 2010, **51**, 3054-3063.
30. J. N. Israelachvili, *Intermolecular and surface forces*, Academic Press, Amsterdam, 3rd edn., 2011.
31. A. Lozsan, M. Garcia-Sucre and G. Urbina-Villalba, *Phys. Rev. E*, 2005, **72**.
32. B. Vincent, J. Edwards, S. Emmett and A. Jones, *Colloid Surface*, 1986, **18**, 261-281.
33. B. L. T. Lau, W. C. Hockaday, K. Ikuma, O. Furman and A. W. Decho, *Colloid Surface A*, 2013, **435**, 22-27.
34. D. P. Stankus, S. E. Lohse, J. E. Hutchison and J. A. Nason, *Environ. Sci. Technol.*, 2011, **45**, 3238-3244.
35. M. C. Surette and J. A. Nason, *Environ. Sci.: Nano*, 2016, **3**, 1144-1152.
36. E. Fischer, *EPA Newsletter*, 1984, **21**, 33-34.
37. V. A. Hackley and J. D. Clogston, *Measuring the size of nanoparticles in aqueous media using batch-mode dynamic light scattering*, Report Special Publication (NIST SP) - 1200-6, Nanotechnology Characterization Laboratory; National Institute of Standards and Technology, 2015.
38. S. Guha, M. Li, M. J. Tarlov and M. R. Zachariah, *Trends Biotechnol.*, 2012, **30**, 291-300.
39. R. Kretzschmar, H. Holthoff and H. Sticher, *J. Colloid Interf. Sci.*, 1998, **202**, 95-103.
40. H. Holthoff, S. U. Egelhaaf, M. Borkovec, P. Schurtenberger and H. Sticher, *Langmuir*, 1996, **12**, 5541-5549.
41. P. C. Hiemenz and R. Rajagopalana, *Principles of colloid and surface chemistry*, CRC Press, Boca Raton, 3rd edn., 1997.
42. K. Rahme, L. Chen, R. G. Hobbs, M. A. Morris, C. O'Driscoll and J. D. Holmes, *RSC Adv.*, 2013, **3**, 6085-6094.
43. Y. Borodko, S. E. Habas, M. Koebel, P. D. Yang, H. Frei and G. A. Somorjai, *J. Phys. Chem. B*, 2006, **110**, 23052-23059.
44. T. Fouquet, M. Torimura and H. Sato, *Mass Spectrom.*, 2016, **5**, A0050-A0050.
45. W. Zhang, Y. Li, J. F. Niu and Y. S. Chen, *Langmuir*, 2013, **29**, 4647-4651.
46. C. M. Lee and W. D. Kumler, *J. Am. Chem. Soc.*, 1961, **83**, 4586-4590.
47. C. M. Lee and W. D. Kumler, *J. Am. Chem. Soc.*, 1961, **83**, 4593-4596.
48. Lanxess., in *Baypure: General product information*, 2005, p. 33.
49. Sigma-Aldrich, *Product specification: Polyvinylpyrrolidone - average mol wt 40,000*, Report Specification PRD.0.ZQ5.10000015954.
50. Y. Li, W. Zhang, J. F. Niu and Y. S. Chen, *ACS Nano*, 2012, **6**, 5164-5173.
51. M. Misawa and J. Takahashi, *Nanomed. Nanotechnol. Biol. Med.*, 2011, **7**, 604-614.
52. R. X. Huang, R. P. Carney, F. Stellacci and B. L. T. Lau, *Langmuir*, 2013, **29**, 11560-11566.
53. R. X. Huang, R. R. Carney, K. Ikuma, F. Stellacci and B. L. T. Lau, *ACS Nano*, 2014, **8**, 5402-5412.

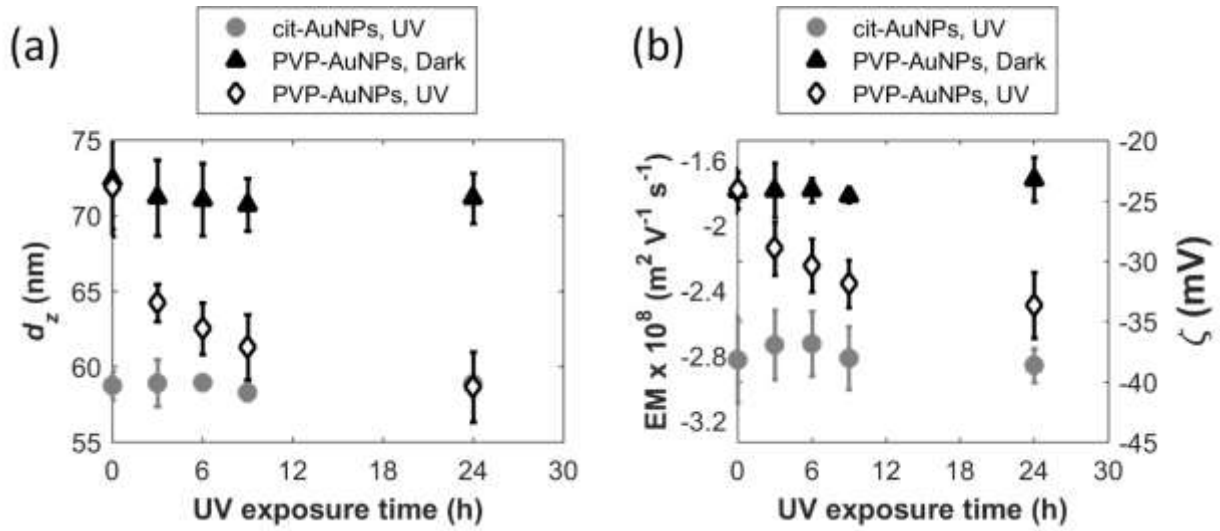

Figure 1. (a) Hydrodynamic diameter of the hydrated PVP-AuNPs (by DLS) and (b) EM of the PVP-AuNPs both decrease significantly over 24 h of UV exposure. Measurements were collected on ≈ 2.8 mg L^{-1} AuNPs in 0.9 mmol L^{-1} $NaHCO_3$ in water at pH 8. Error bars represent the standard deviation of 3 or more measurements on independently prepared AuNPs.

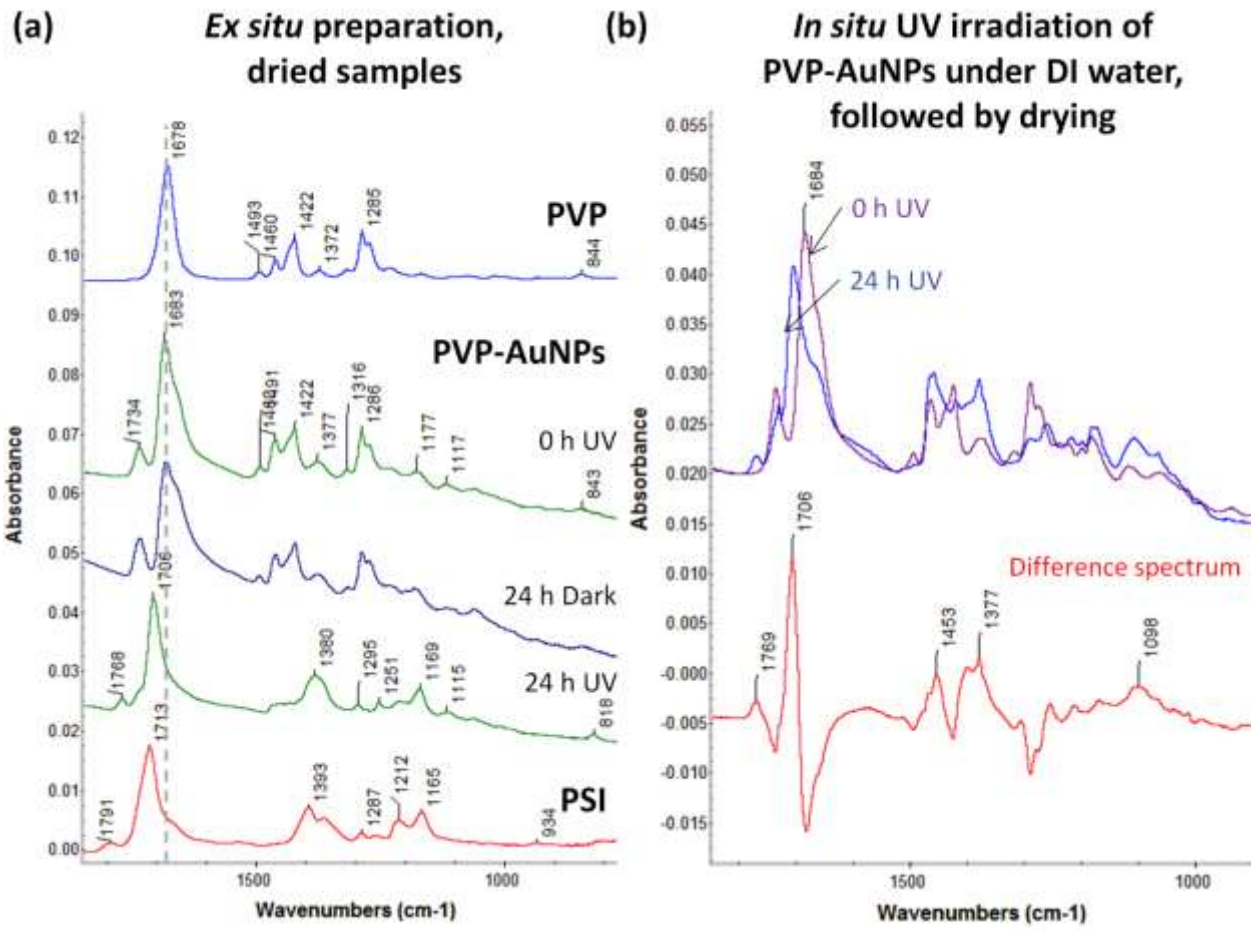

Figure 2. ATR-FTIR absorbance spectra collected on (a) PVP-AuNPs and the PVP and PSI polymer controls (without AuNPs) prepared *ex situ* and dried for analysis, and (b) PVP-AuNPs dried on the diamond ATR substrate as-prepared (0 h UV) and after 24 h of UV irradiation *in situ* under DI water, followed by removal of the water overlayer and drying of the AuNP film (24 h UV). Methods for the *in situ* experiments are described in the SI. Background spectra were obtained on the clean diamond substrate. The difference spectrum in (b) is obtained by subtracting the 0 h UV spectrum from the 24 h UV spectrum. In (a), spectra are shown at different absorbance scales for visual clarity; in (b), all spectra are set to a common absorbance scale (i.e., relative peak heights are comparable) but vertically shifted along the *y*-axis. Spectra are the result of averaging 250 scans on one sample. Duplicate samples were analyzed for both (a) and (b) and yielded consistent results (not shown).

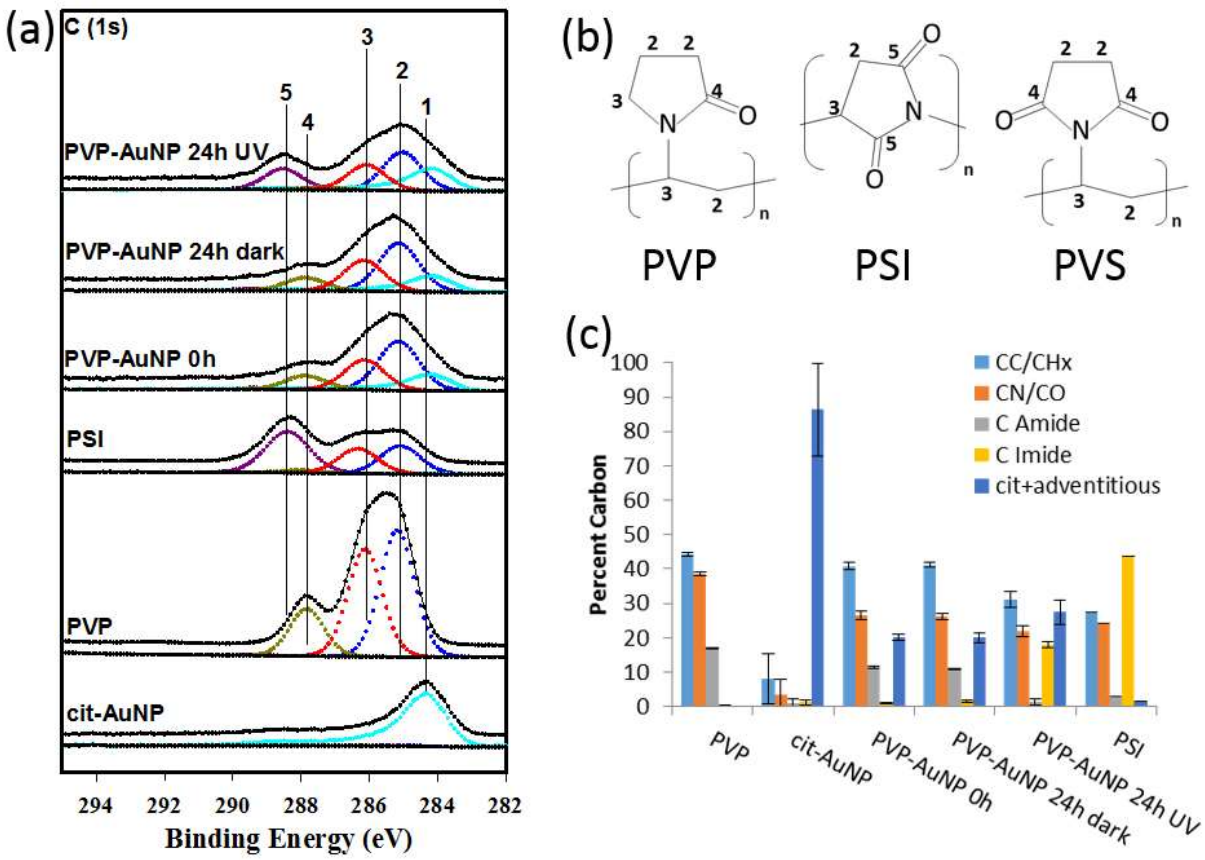

Figure 3. Results from XPS data analysis for C 1s spectra. (a) Peak fitted spectra representative of all PVP-AuNP samples and controls. Fits for the C(1s) region represent 1. Trace citrate and adventitious carbon; 2. hydrocarbon/aromatics (CC/CH_x); 3. C bound to 1 N (CN); 4. amide; and 5. imide carbon. (b) Models of polymer controls PVP, PSI, and theorized product, PVS, with each carbon labelled consistent with Figure 4(a). (c) Percent contributions to the C(1s) region for PVP-AuNP and controls. Error bars represent standard deviations of measurements from three or more spots on a single sample with the exception of the PSI sample which is representative of only one measurement.

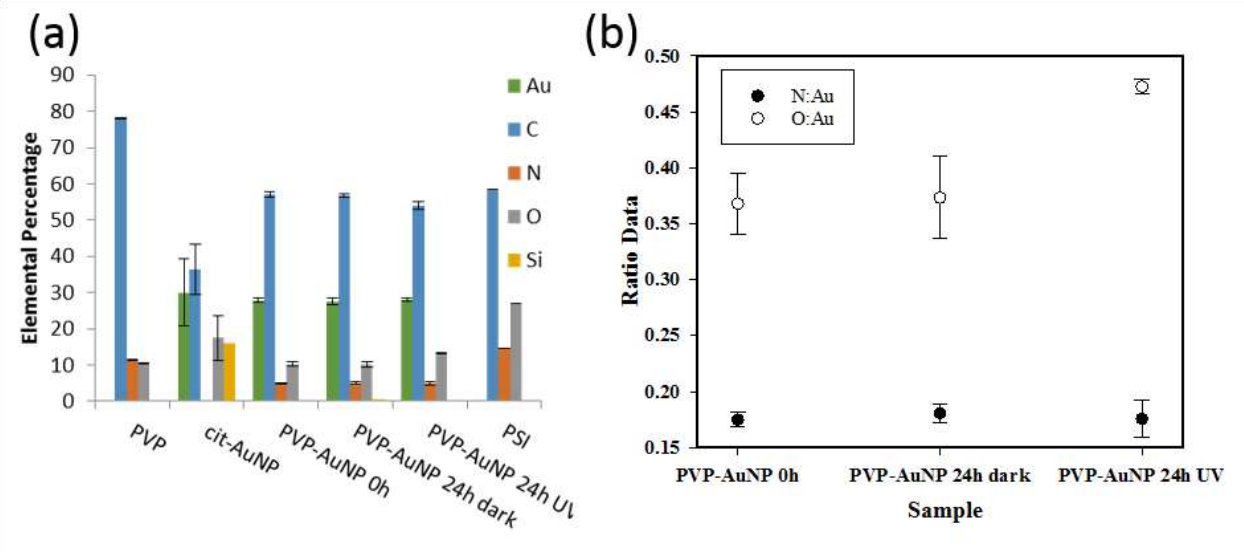

Figure 4. (a) Elemental percentages of the PVP-AuNP experiments and controls. (b) Ratio of elemental compositions for PVP-AuNP samples. The Si contribution on the cit-AuNP sample is from the silicon wafer used as the substrate (for all other samples, sufficient AuNP coverage was achieved such that Si was not observed). Error bars represent standard deviations of measurements from three or more spots on a single sample with the exception of the PSI sample which is representative of only one measurement.

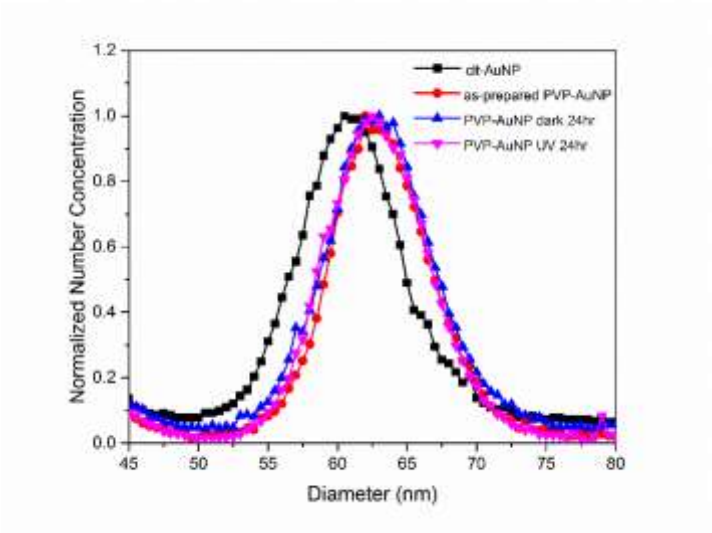

Figure 5. ES-DMA size distributions of the aerosolized (dry) PVP-AuNPs after 24 h UV irradiation, in comparison to the 24 h dark control, as-prepared PVP-AuNPs (0 h UV), and cit-AuNPs. Duplicate measurements were collected on each sample (not shown) and were similar to those shown here.

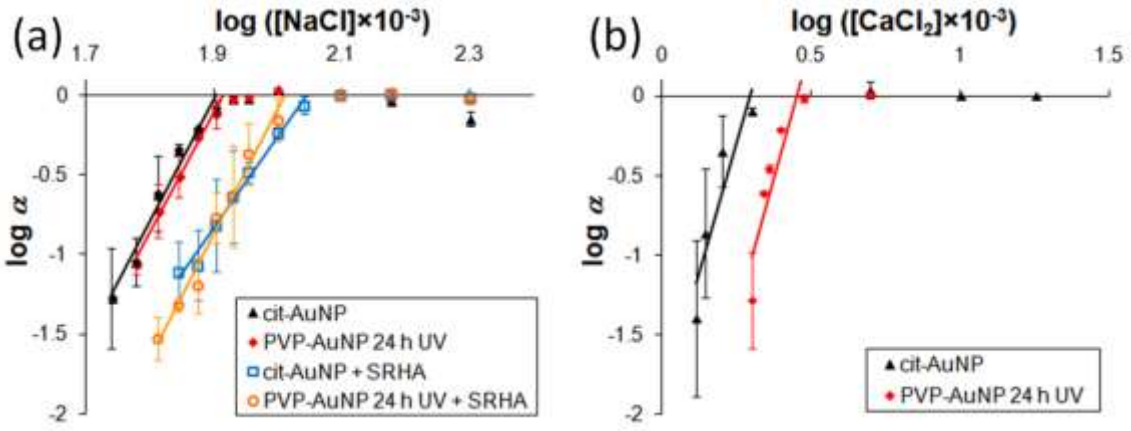

Figure 6. Attachment efficiencies of the UV-exposed PVP-AuNPs and cit-AuNPs (before or after equilibration in 8 mg L^{-1} SRHA) in NaCl (a) and $CaCl_2$ (b) for determination of the CCC. Attachment efficiencies were determined by dividing rates of change in d_z during the initial stage of aggregation (dimer formation) by the average rate for samples in the diffusion-limited aggregation regime. Lines of best fit are drawn through points below the CCC to determine the CCC from the *x*-intercept. All samples included 1 mmol L^{-1} $NaHCO_3$ and were at pH 8. Error bars represent standard deviations of measurements on at least 2 independently prepared samples.

Table 1. Comparison of photo-transformation outcomes for mPEGSH[25] and PVP coatings

	mPEGSH-AuNPs[25]	**PVP-AuNPs**
Layer thickness	Decrease in hydrated layer thickness of coating	
Adsorbed mass / structure	Nearly complete loss (detachment) of ether chain	Layer collapse with no detectable loss of coating mass
Residual coating	Detectable persistence of transformation products on AuNPs	
	Thiolated fragment	Oxidized product (postulated imide)
Colloidal stability	Loss of steric stabilization in NaCl, MHW, and ASW	Loss of stabilization in NaCl; only partial loss of stabilization in $CaCl_2$
Predictability from pure polymer studies (without NPs)	Only intermediate transformation products observed on AuNPs after 24 h	
	No observable oxidation or desorption of thiolate from AuNPs	No observable hydrolysis or loss by scission on AuNPs